Microchimica Acta (2022) 189: 304
https://doi.org/10.1007/s00604-022-05380-9

ORIGINAL PAPER

Accurate identification of kidney injury progression via a fluorescent biosensor array

Xie-an Yu[1,2] · Lei Zhang[1] · Ran Zhang[1] · Xuefei Bai[1] · Ying Zhang[1] · Yiting Hu[1] · Yang Wu[1] · Ziyi Li[1] · Bing Wang[2] · Jiangwei Tian[1]

Received: 26 October 2021 / Accepted: 26 June 2022 / Published online: 1 August 2022

Abstract

Identifying the progress of kidney injury may aid the effective treatment and intervention. Herein, we developed a fluorescent biosensor array for instantaneous and accurate identification of the kidney injury progression via "doubled" signals. The multichannel biosensor array consisted of polydopamine-polyethyleneimine (PDA-PEI) and multicolor-labelled different length of DNAs including AAAAA-Cyanine7 (5A-Cy7), AAAAAAAAAA-Texas Red (10A-Texas Red), and AAAAAAAAAAAAAAAAAA-VIC (20A-VIC). Facing to the variety of protein in urine with alterable charge accompanied with different progress of kidney injury, the composition of urine replaces the DNA signal molecules, forming their special fluorescence patterns. Taking the size of protein into consideration, the original three variables induced by the protein charge were extended to six variables induced by the two factors of protein particle size and charge difference, which could provide a more accurate strategy to identify the progress of kidney injury. Notably, this strategy not only opened up new perspective for identification the progress of kidney injury via the size and charge of urine protein, but also improved the resolving power of sensor array by increasing the number of sensor elements for extending their potential application to various diseases.

Keywords Proteinuria · Charge and size of urine protein · Multichannel biosensor array · Two-dimensional amplification

Introduction

Insight into the progress of kidney disease can summarize that kidney failure is the end stage of kidney injury and may require treatment by dialysis or transplantation [1–4]. Accordingly, identification the different progress of kidney injury may aid the effective treatment and intervention [5–8]. Facing to the current challenge for staging the kidney disease, different criteria have been attempted previously making it possible to reach accurate conclusions on the epidemiology of syndromes. For acute kidney injury (AKI), there were a consensus definition called RIFLE (risk, injury, failure, loss, and end) criteria, which could be used to standardize and classify renal dysfunction indicated [9]. As for chronic kidney disease (CKD), glomerular filtration rate (GFR), albuminuria, and novel urine biomarkers such as cystatin C (Cys C) were also used to evaluate the development of CKD [10]. Indeed, these criteria main used GFR, generally reflected by measuring serum creatinine and urine output, to define and stage AKI and CKD. Nevertheless, the delay ability and low specificity of serum creatinine and the inconvenience for collecting urine output for 12 h have brought challenges to accurate and rapid determination the progress of AKI and CKD [11–13]. Besides, single urine biomarker was encouraging but relatively imprecise and far from definitive. Thus, taking albuminuria into consideration, the staging and

Xie-an Yu and Lei Zhang contributed equally to this work.

✉ Bing Wang
wangbing@szidc.org.cn

✉ Jiangwei Tian
jwtian@cpu.edu.cn

[1] State Key Laboratory of Natural Medicines, Jiangsu Key Laboratory of TCM Evaluation and Translational Research, Research Center for Traceability and Standardization of TCMs, School of Traditional Chinese Pharmacy, China Pharmaceutical University, Nanjing 211198, People's Republic of China

[2] NMPA Key Laboratory for Bioequivalence Research of Generic Drug Evaluation, Shenzhen Institute for Drug Control, Shenzhen 518057, People's Republic of China

classifying of kidney disease would be more accurate and reliable. Exploring the kidney's excretory function further, glomerular filtration membrane as a glomerular filtration barrier was not only a "size cutoff" slit but also preferred to negative charge of protein in a normal physiological state [14, 15]. Accordingly, the different levels of kidney damage would induce the diverse albuminuria with various size and disparate charge.

Array-based sensing protocols with feature of rapidly profiling complex chemical and biological systems rose in response to the proper time and conditions for the intricate albuminuria [16–20]. The selective interaction between signal molecule and proteins could generate a complex protein-specific and simple signature pattern, which was instantaneously produced to discriminate biological sample [21–25]. However, few variables of fluorescent biosensor array may raise concerns about their application in accurate classification of kidney disease. Hence, extending the number of signal molecules would improve the accuracy of fluorescent biosensor array.

Huangkui (HK) capsule that could treat chronic glomerulonephritis, diabetic nephropathy, nephrotic syndrome, and other chronic kidney diseases has been approved by the China State Food and Drug Administration (Z19990040) for the treatment of nephritis [26, 27]. Therefore, the HK capsule can be used as a model drug to test the feasibility of fluorescent biosensor array for the identification of kidney injury progression.

Herein, given an insight into the size and charge of urine protein, two key elements of glomerular filtration barrier, a multichannel biosensor array was developed for instantaneous and accurate identification the progress of kidney injury via "doubled" the signals. As was illustrated in Scheme 1, the multichannel biosensor was constructed by polydopamine-polyethyleneimine (PDA-PEI) with positive charge and multiwavelength-labelled different length of DNAs with negative charge via noncovalent conjugation such as electrostatic and π–π stacking. With an increasing number of DNA base, the binding capacity to PDA-PEI was also improved. Moreover, DNAs synthesized and labeled with multiwavelength-fluorophore contained properties of low cost, high purity, and robust stability. The fluorophore-labelled DNAs were absorbed on the surface of the PDA-PEI due to the non-covalent interaction such as π–π stacking and hydrogen bonding between the DNAs and PDA-PEI, forming a PDA-PEI/DNAs nanocomplex and enabling fluorescence quenching via the Förster resonance energy transfer (FRET) principle [28]. Exploitation of these potencies would spawn the three signal molecules of this biosensor, that was AAAAA-Cyanine7 (5A-Cy7), AAAAAAAAAA-Texas Red (10A-Texas Red) and AAA AAAAAAAAAAAAAAAA-VIC (20A-VIC), respectively. In the presence of urine containing various proteins with different charge, the binding equilibrium between DNAs and PDA-PEI was broken and the binding between urinary proteins and PDA-PEI took place, resulting in a rapid displacement of DNAs from the surface of PDA-PEI [29]. Initially, the urine of unilateral ureteral occlusion (UUO) mice for 14 days was collected and generated their corresponding "signature"-based on profiling of the output of sensor array. The specific data of three signal molecules was quantitatively interpreted using principal component analysis (PCA), partial least-squares discrimination analysis (PLS-DA), and linear discriminant analysis (LDA) [30–32]. Consequently, four distinct clusters arising from urine of UUO mice collected 0–14 day was revealed according to the different progress of kidney injury. This strategy was also applied to cisplatin-induced AKI mice and clinical diabetic nephropathy, successfully staging and classifying the renal dysfunction. Furthermore, it was well known that the number of sensing elements was closely related to the resolving power and discrimination ability of a sensor array. Hence, introducing the size of protein, another key element of urine protein, ultrafiltration centrifuge can obtain the small and big size of the urine protein, forming the double signals of this sensor array. The double signals with the output channels of six was obtained, which could provide a more accurate strategy to identify the progress of kidney injury. Comparing to three channels of sensor array, the increased information content of double signals induced the urine of UUO mice to seven distinct clusters, allowing facile and accurate discrimination of the progress of kidney injury. Besides, PDA-PEI/DNA sensor was also helpful for evaluation of the therapeutic effect of HK capsule for kidney injury, which demonstrated that HK capsule could relieve the progression of kidney injury effectively. Notably, this strategy not only opens up new perspective for identification the progress of kidney injury via the size and charge of urine protein but also improves the resolving power of sensor array by increasing the number of sensor elements for extending their potential application in various diseases.

Experimental section

Materials and reagents

Dopamine hydrochloride (DA·HCl) was offered by Solarbio Biotechnology Co., Ltd. (Beijing, China). Polyethyleneimine (PEI, M.W. 1800) was purchased from Macklin Biochemical Co., Ltd. (Shanghai, China). Different DNA signal molecule 5A-Cy7, 10A-Texas Red and 20A-VIC were synthesized by Shanghai Sangon Biotechnology Co. (Shanghai, China). Cisplatin was provided by Liangwei Biotechnology Co., Ltd. Ultrapure water (electric resistance > 18.25

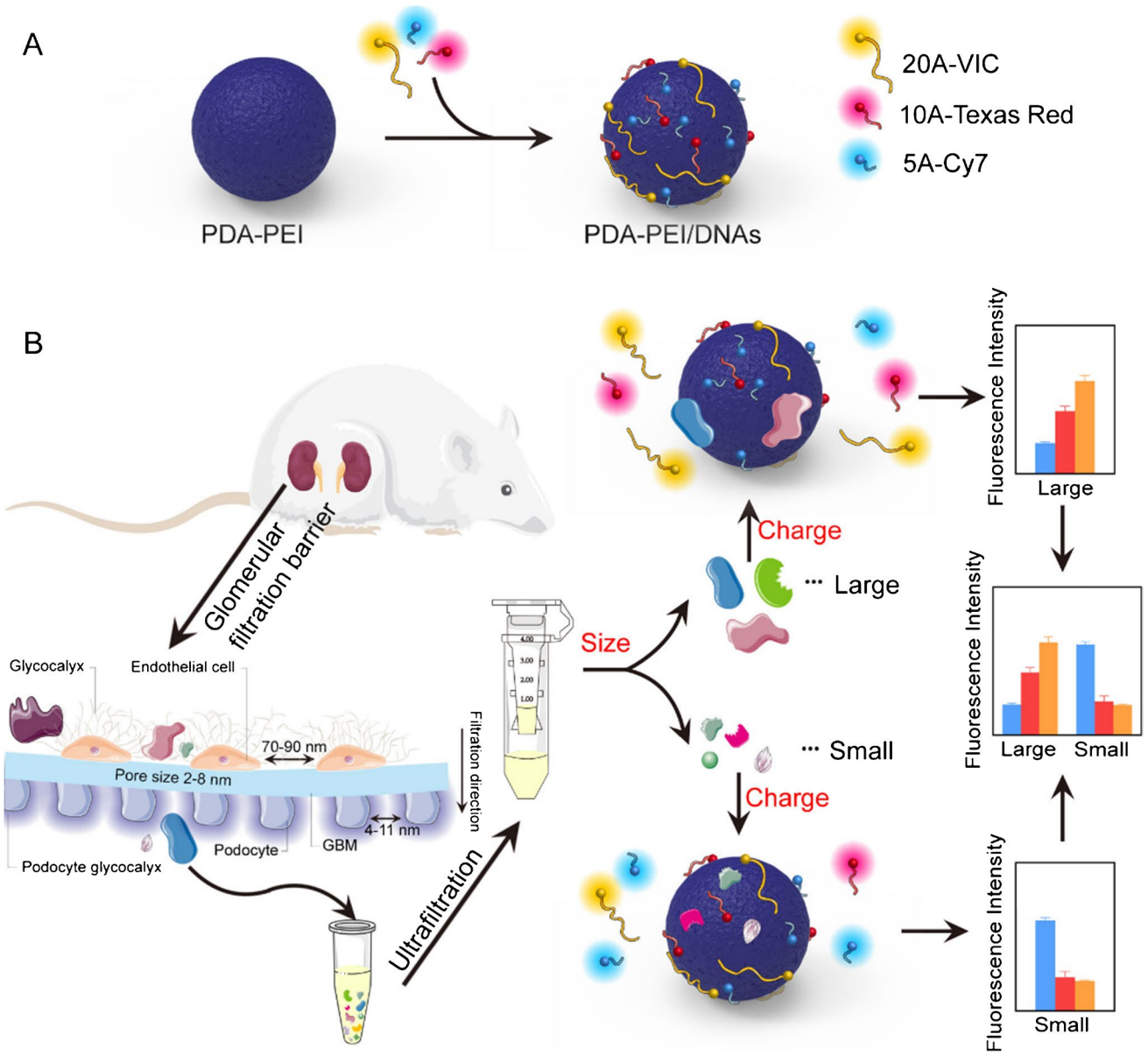

Scheme 1 Schematic illustration of **A** the construction of the PDA-PEI/DNAs sensor and **B** the application of the PDA-PEI/DNAs sensor in monitoring and evaluating the process of kidney injury

MΩ·cm) produced by a Millipore Milli-Q water purification system (Billerica, MA, U.S.A.) was used throughout the experiments.

Instruments

The absorption spectra of DA, PEI and PDA-PEI were recorded on a Cary Series UV–vis spectrophotometer (Agilent Technologies, USA). The excitation and emission spectra of 5A-Cy7, 10A-Texas Red, and 20A-VIC were collected by Cary Eclipse Fluorescence Spectrophotometer (Agilent Technologies Inc., USA). The morphology of PDA-PEI was featured at a JEOL JEM-200CX transmission electron microscope (TEM) worked at 200 kV. The size of PDA-PEI was measured by dynamic light scattering (DLS) via a Mastersizer 2000 particle size analyzer. The zeta potential was assayed on a Malvern Zeta sizer-Nano Z instrument (Nano-Z, Malvern, UK). Bruker Tensor 27 FTIR spectrometer was used to measure the Fourier transform infrared (FT-IR) spectra of DA, PEI, and PDA-PEI. The detailed fluorescence intensity was gained by Varioskan Flash (Thermo Scientific, USA). Hematein eosin (HE) and Masson staining images were amplified on a digital pathology slice scanner using NanoZoomer 2.0 RS (Hamama-tsu, China).

Synthesis and characterization of PDA-PEI/DNAs sensor

PDA-PEI carrier was prepared by coploymerization of DA and PEI [33–36]. Briefly, 10 mg DA·HCl and 10 mg PEI were dissolved in 10 mL Tris–HCl buffer (10 mM, pH 7.4). Then, the solution was stirred on a magnetic stirrer to react fully for 2 h. Following, the obtained solution was further processed with dialysis tube. Finally, the PDA-PEI copolymer was collected and stored at 4 °C for further use. Adding different concentration of DNAs to PDA-PEI, PDA-PEI/DNAs sensor was obtained via the noncovalent conjugation such as electrostatic and π–π stacking.

Fluorescence titrations of DNA signal molecule by PDA-PEI

Each type of DNA signal molecule with concentration of 100 nM was separately titrated by different concentration of PDA-PEI ranged from 0 to 250 ng mL^{-1}. Then, the fluorescence intensity of 5A-Cy7, 10A-Texas Red and 20A-VIC with different concentrations of PDA-PEI were recorded at the excitation/emission wavelengths of 735/755 nm, 590/615 nm, and 535/555 nm, respectively. Subsequently, the quenching efficiency was calculated as follows: quenching efficiency (%) = $100 \times (F_0\text{-}F_n)/F_0$, where F_0 represented the fluorescence intensity of DNA signal molecule, and F_n was the fluorescence intensity of them after adding various concentrations of PDA-PEI. Finally, nonlinear least-squares curve fitting analysis was adopted to evaluate the binding constant (K_a) of PDA-PEI/DNAs complex.

Establishment of kidney injury model in mice

The male ICR mice weighted 20–24 g were purchased from the Laboratory Animal Center and Institute of Comparative Medicine at Yangzhou University. The mice were bred in an axenic environment, maintained at the temperature of 25 °C, housed with a 12-h light/dark cycle, and allowed free access to food and water. All animal operations were according with institutional animal use and care regulations approved by the Model Animal Research Center of China Pharmaceutical University.

The AKI model was induced by intraperitoneal injection of Cisplatin at the dosage of 5 mg kg^{-1} for 7 days [37–39]. Then, the urine of mice was collected every day and storied at − 20 °C for the further experiment.

The UUO mouth was a well-known model for CKD. According to the literature, the mice were anesthetized by intraperitoneal injection of 1% sodium pentobarbital and put on the operating table. Then, the left abdomen was opened to expose the left kidney. Following that, the ureter was exposed and double ligated with suture. Finally, the incision was sutured layer by layer with disinfection of iodophor. The urine of UUO mice were collected daily for 14 days and stored in a fridge at − 20 °C for the further experiment.

The urine samples of clinical diabetic nephropathy were offered by Jiangsu Province Hospital of Chinese Medicine. All procedures were approved by the medical ethics committee of the Jiangsu Province Hospital of Chinese Medicine and followed the tenets of the Declaration of Helsinki.

Statistical analysis

All experiment parameters were tested at least three times. GraphPad Prism and Origin software were employed for statistical analysis. SPSS and SIMCAP software were used to carry out the PCA, PLS-DA and LDA analysis.

Results and discussion

Characterization of PDA-PEI/DNAs

The PDA-PEI was synthesized via Michael addition with DA and PEI under the mild conditions. The TEM image (Fig. 1A) showed the successful synthesis of PDA-PEI with the characteristic of spherical, uniform in size and homogeneous-dispersed. DLS results indicated that the average size of PDA-PEI was nearly 290 nm (Fig. S1). Also, the DLS results of PDA-PEI/DNAs demonstrated that the hydrodynamic diameter increased to 302 nm (Fig. S2), indirectly illustrating DNAs binding on the surface of PDA-PEI. The zeta potential of PDA-PEI was + 22.4 mV (Fig. 1B), indicating the positive polarity of PDA-PEI. Whereas the PDA-PEI/DNAs hold the positive charge of + 8.5 mV (Fig. S3), which could be served as extra information for the negative charge DNAs conjugated to PDA-PEI via electrostatic interaction. Focused on the UV–visible spectroscopy, the absorption spectroscopy of the PDA-PEI presented two characteristic peaks at about 280 nm and 380 nm (Fig. 1C). Comparing to the absorption spectrum of DA with only a characteristic broaden absorbance peak at 280 nm, the peak of PDA-PEI at 380 nm was the characteristic peak of the Michael adduct. Moreover, the appearance of broad bands around 3300 cm^{-1} was attributed to -OH and -NH groups of PDA–PEI, which confirmed the composite formation with PEI (Fig. 1D). Also, the peak at 1650 cm^{-1} was determined to the $\nu_{C=N}$ vibration, further proving the successful cross-linking of PEI and PDA. As for the stability of the PDA-PEI, the results showed that the fluctuation of size and zeta potential was almost neglected (Figs. S4 and S5),

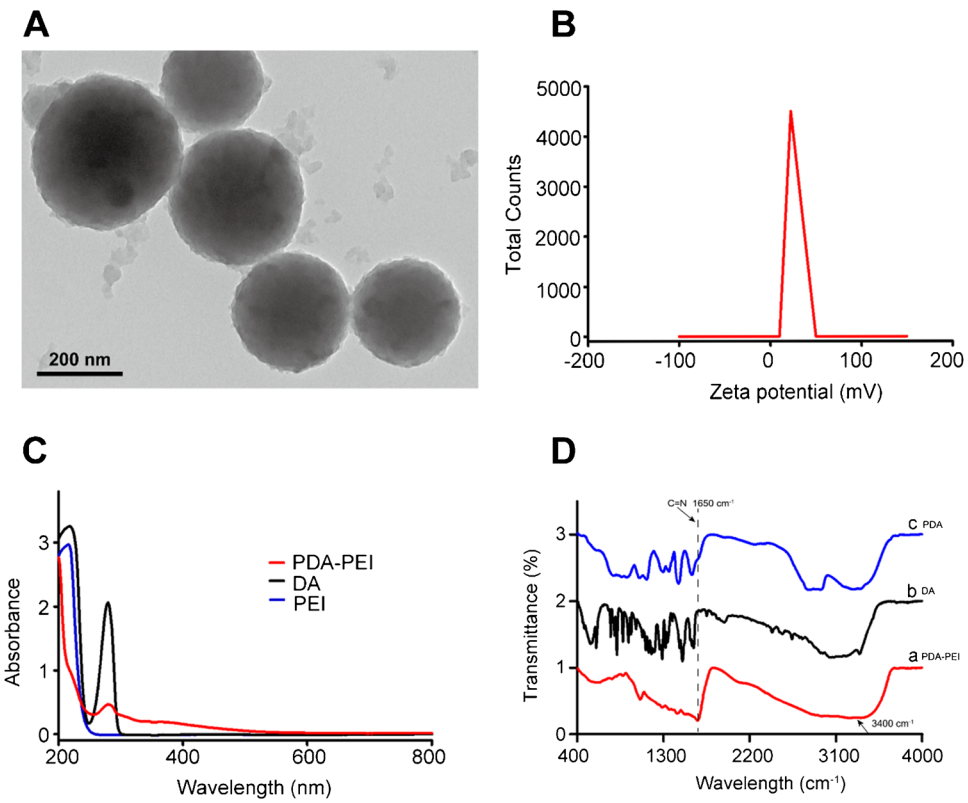

Fig. 1 **A** TEM image and **B** zeta potential of PDA-PEI. **C** UV–vis absorption spectrum of PDA-PEI, DA and PEI. **D** FTIR spectrum of (a) PDA-PEI, (b) DA, and (c) PDA

indicating the good stability of PDA-PEI. Taking together, the above results demonstrated the successful synthesis of PDA-PEI.

Fluorescence titrations

Fluorescence spectra of DNAs manifested that the optimal excitation/emission wavelengths of 20A-VIC, 10A-Texas, and 5A-Cy7 were 535/555, 590/615, and 735/755 nm, respectively, providing an independent fluorescence response from every channel without cross-interference (Fig. 2A). Since the binding thermodynamics of the PDA-PEI/DNAs biosensor was critical in the sensing mechanism, the association constants of PDA-PEI toward three DNAs were explored for profiling the various output of sensor array. Fluorescence titration spectra revealed that the fluorescence of DNAs was gradually quenched with an increasing concentration of PDA-PEI (Fig. 2B). The nonlinear least square fitting curve was utilized to analyze corresponding binding constants between each DNA and PDA-PEI. As a result, the affinity varied significantly with the order of 20A-VIC > 10A-Texas Red > 5A-Cy7 (Table S1), revealing that the differential fluorescence signals could be generated owing to the selective combination between the biosensor and multiple analytes. Moreover, the titration experiment revealed that the fluorescence quenching was saturated when the ratio of [PDA-PEI]/[ssDNA] reached 2.5. To eliminate interactions between different signaling molecules, 250 ng mL^{-1} PDA-PEI and 100 nM DNAs were chosen to correspond to the inflection point observed in the fitting curve. Moreover, fluorescence lifetime was measured to explore the fluorescence quenching mechanism between PDA-PEI and DNAs. As was shown in Fig. S6, the lifetime of the DNAs decreased from 7.13 ns to 2.42 ns after interacting with PDA-PEI, indicating that the quenching mechanism of the DNAs and PDA-PEI was dynamic quenching. Subsequently, we use some proteins including bovine serum albumin (BSA), human serum albumin (HAS), and cystatin C (Cys C) to explore the fluorescence recovery of PDA-PEI/DNAs biosensor. As shown in Figs. S7–S9, after the addition of different proteins, the fluorescence intensity of PDA-PEI/DNAs biosensor displayed different degrees of recovery, which verified the feasibility of the sensor for urine protein recognition. What is more, the fluorescence intensity of 5A-Cy7, 10A-Texas Red and 20A-VIC showed a linear relationship with the concentration of BSA in the range of 10 to 500 ng mL^{-1} (Figs. S10–S12), and the limit of detection (LOD) was 40.51 g mL^{-1}, 41.70 g mL^{-1}, and 47.09 g mL^{-1}, respectively, which was calculated according to the equation $LOD = 3S_b/m$, where S_b was the standard deviation of the blank measurements and m was the slope of the calibration curve. These results confirmed the adaptability of the fluorescent biosensor for selective and sensitive detection of urinary proteins. In addition, the stability studies of

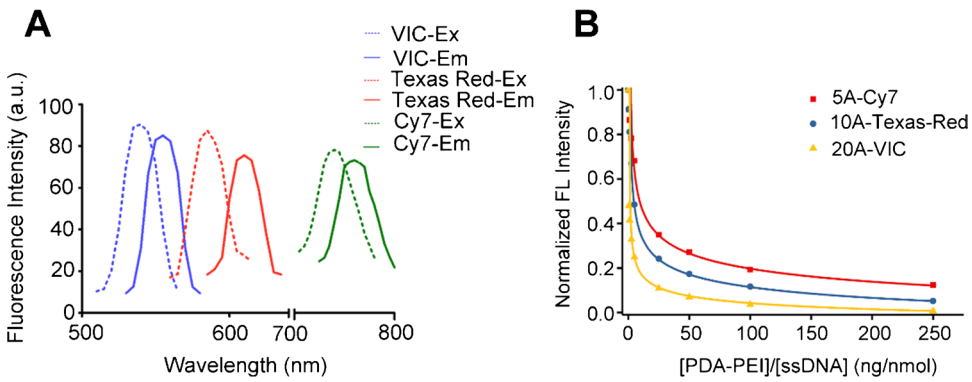

Fig. 2 **A** Excitation and emission wavelengths of 20A-VIC, 10A-Texas Red, and 5A-Cy7. **B** Fluorescence titration of 20A-VIC, 10A-Texas Red, and 5A-Cy7 by PDA-PEI

PDA-PEI/DNAs biosensor were also evaluated. As shown in Figs. S13–S18, the fluorescence intensity of 5A-Cy7, 10A-Texas Red, and 20A-VIC remained stable after adding PDA-PEI at 1 min, 5 min, 1 h, 2 h, 24 h, 48 h, and 72 h, illustrating the good stability of PDA-PEI/DNA biosensor in PBS and serum. It was worth noting that the fluorescence intensity of PDA-PEI/DNAs increased in serum due to the presence of serum protein. But the fluorescence intensity of PDA-PEI/DNAs still remained stable after incubation for different days, which further demonstrated the good stability of PDA-PEI/DNAs biosensor.

Discrimination the progress of cisplatin-induced AKI model

Three DNAs presenting differentiated binding affinity with PDA-PEI were used to build the multichannel sensor to obtain an information-rich output from a single measurement and reproducible sensor responses. Subsequently, the AKI mice model was constructed by intraperitoneal injection of cisplatin and two clinical biomarkers including neutrophil gelatinase-associated lipocalin (NGAL) and cystatin C (Cys C) are provided in Figs. S19 and S20. With an increase in the time of AKI induced by cisplatin, the concentration of NGAL and Cys C increased obviously, which confirmed the successful establishment of AKI mice model. After optimizing the composition of the sensor and constructing the AKI mice model successfully, the obtained corresponding "signature" of the mice urine given the Cisplatin for different days are shown in Fig. 3A and Table S2. It was noticed that different days of cisplatin injection resulted in different charges of urinary protein, leading to the various binding forces between urinary protein and the sensor and changes in fluorescence intensity. In order to preliminarily distinguish the degree of cisplatin-induced kidney injury, PCA was employed to identify the fluorescence response pattern (Fig. S21). Under the unsupervised mode, the urine of mice given cisplatin for different days was divided into six groups, which respectively represented the response pattern for an individual injury stage induced by cisplatin. In addition, the fitting parameters of PCA model were $R^2 = 0.968$, $Q^2 = 0.854$, respectively. The closer R^2 was to 1, the more stable the model was. $Q^2 > 0.5$ indicated the higher prediction accuracy of the model. On the basis of PCA grouping results, PLS-DA and LDA were validated again to quantify the fluorescence response. It was worth noting that days 0, 1, 2, 3, 4, and 5 to 6 of the six groups were significantly separated (Fig. 3B), which indicated that the proposed method can be used to rapidly identify the developmental course of cisplatin-induced kidney injury. LDA model performance was measured in terms of precision, sensitivity, specificity, and accuracy of calibration model [40, 41]. Values of precision, sensitivity, and selectivity are equal to 1.00 and accuracy of 100% show good discriminative power (Table S3). The grouping results of PLS-DA (Fig. S22) were consistent with those of PCA. Meanwhile, we further quantified the grouping condition according to the results of LDA analysis, the linear discriminant function constructed with three variables as indicators were as follows:

$$Y_1 = 4.398X_1 + 11.464X_2 + 0.338X_3 - 634.263$$
$$Y_2 = 3.488X_1 + 12.083X_2 + 0.365X_3 - 655.456$$
$$Y_3 = 4.884X_1 + 13.214X_2 + 0.494X_3 - 851.468$$
$$Y_4 = 5.345X_1 + 13.917X_2 + 0.453X_3 - 942.266$$
$$Y_5 = 6.310X_1 + 13.227X_2 + 0.579X_3 - 950.204$$
$$Y_6 = 3.843X_1 + 13.042X_2 + 0.532X_3 - 791.283$$

where Y_1–Y_6 respectively denote the damage process of cisplatin-induced kidney injury mice in 0, 1, 2, 3, 4, and 5–6 days, and X_1–X_3 represent the fluorescence intensity of three signal molecules. The value of fluorescence signal induced by urine samples with unknown kidney damage degree was directly brought into the constructed discriminant function and classified into its grouping. Consequently, the developmental course of kidney injury can be quickly identified. Additionally, the hematoxylin–eosin staining (H&E) method was used to further verify the rationality of

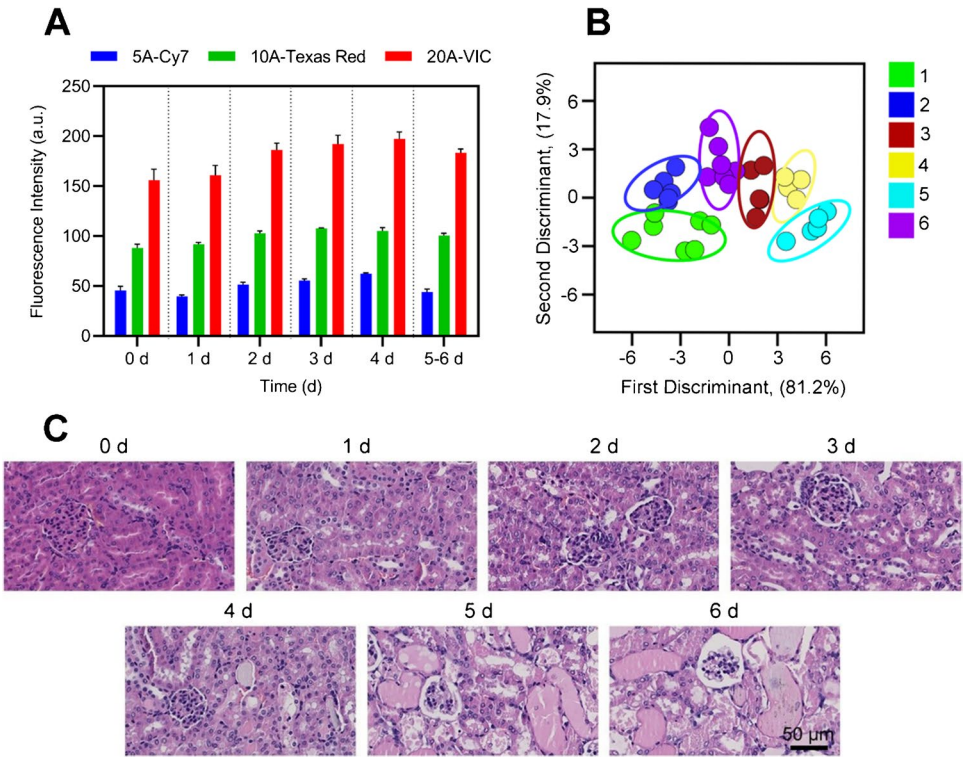

Fig. 3 **A** Fluorescence response patterns generated by PDA-PEI/DNAs sensor array for identifying the different kidney injury degrees induced by cisplatin. **B** LDA score for discrimination of cisplatin-induced kidney injury: 1, control group; 2, administration of cisplatin for 1 day; 3, administration of cisplatin lasted 2 days; 4, administration of cisplatin lasted 3 days; 5, administration of cisplatin lasted 4 days; 6, administration of cisplatin lasted 5–6 days. **C** The H&E staining imaging of renal tissue from cisplatin-induced kidney injury model for different administrated days. Scale bar: 50 μm

the constructed group (Fig. 3C). With the increase of the days of cisplatin administration, the glomerulus gradually atrophied, the renal tubules showed significant degeneration and a large amount of proteinuria was seen in the necrotic renal tubules. The above results illustrated that the degree of kidney damage gradually increased with the days of cisplatin administration, which further supported that there was correlation between the development process of kidney injury in disparate stages and the fluorescence response obtained through the sensor. Generally, all of the above results demonstrated the rationality of the constructed multichannel biosensor array in the identification of the development process of cisplatin-induced acute kidney injury.

Discrimination and evaluation the progress of UUO model

The UUO mice model was established to further evaluate the application potential of sensor in different scopes. The urine of UUO mice ligated for different days was mixed with the sensor and then placed on a fluorescent microplate to read the fluorescence intensity. As shown in Fig. S23 and Table S4, the fluorescence intensity of the three signal molecules were discrepant after the addition of the urine of UUO mice with different ligation days. PCA analysis showed that the urine of UUO model mice gathered significantly in one group 1–3 days after ligation, in one group 4–7 days after ligation and in another group 8–14 days after ligation (Fig. S24). In addition, the fitting parameters of PCA model were $R^2 = 0.848$, $Q^2 = 0.792$, respectively. The primitively separate results of three classes of ligation days displayed the discrimination ability of PDA-PEI/DNAs sensor. Similarly, according to LDA analysis, the sensors were able to divide the urine of UUO model mice into 4 groups based on ligation days, which were 0 days, 1–3 days, 4–7 days, and 8–14 days, respectively, representing the four stages of the development process of kidney injury (Fig. S25). Values of precision, sensitivity, and selectivity were equal to 1.00 and accuracy of 100% showed good discriminative power (Table S5). The results of PLS-DA divided the samples into four groups in the same way, which were in keeping with the LDA analysis results (Fig. S26). In order to further realize the rapid identification of the developmental degree of kidney injury in unknown samples, a linear discriminant function constructed with three signal molecules as variables were as follows:

$$Y_1 = 5.517X_1 + 0.498X_2 + 2.952X_3 - 342.782$$
$$Y_2 = 5.078X_1 + 0.409X_2 + 3.035X_3 - 323.389$$
$$Y_3 = 5.589X_1 + 0.442X_2 + 3.404X_3 - 399.586$$
$$Y_4 = 6.146X_1 + 0.553X_2 + 3.718X_3 - 485.485$$

where Y_1–Y_4 respectively denote the kidney injury process of UUO mice in 0, 1–3, 4–7, and 8–14 days, and X_1–X_3 represent the fluorescence intensity of three signal molecules.

The fluorescence intensity of three signal molecules induced by the unknown samples was substituted into the constructed linear discriminant function to accurately identify kidney damage degree.

Although based on the change of fluorescence intensity induced by the charge of urine protein, the sensor had been successfully applied in the rapid identification of different processes of kidney injury development in cisplatin-induced acute kidney injury model and UUO model. However, the only three signals were insufficient for accurately discriminating the progress of kidney injury especially for UUO model. Hence, another key element of urine protein, that was size, was introduced to expand variables. The urine protein was classified into the small and big size through ultrafiltration centrifuge, obtaining the urine sample as super layer and under layer. Consequently, the original three variables induced by the protein charge were extended to six variables induced by the double factors of protein particle size and charge difference, aiming to achieve accurate identification of kidney injury progress. As the results, the specific fluorescence intensity of "double" signals is shown in Table S6 and Fig. 4A. Similarly, PCA analysis was performed on the six fluorescence signals induced in the urine of UUO model mice. After increasing the fluorescence signal variables, the urine of UUO model mice was further subdivided into 7 groups (0 days, 1–2 days, 3–4 days, 5–7 days, 8–9 days, 10–11 days, and 12–14 days, respectively), which divided the 8–14 days group into another three groups compared with the grouping results based on only three fluorescence signal variables and refined the overall progression of kidney injury (Fig. S27). In addition, the fitting parameters of PCA model were $R^2 = 0.810$, $Q^2 = 0.740$, respectively. Meanwhile, both PLS-DA (Fig. S28) and LDA (Fig. 4B) successfully divided 14-day UUO model urine into 7 groups, which verified the rationality of the constructed strategy for discriminating the progress the kidney injury via two-dimensional amplification. Values of precision, sensitivity and selectivity were equal to 1.00 and accuracy of 100% showed good discriminative power (Table S7). In order to further quantify the unknown samples, the linear discriminant function was constructed with the six amplified signal molecules as follows:

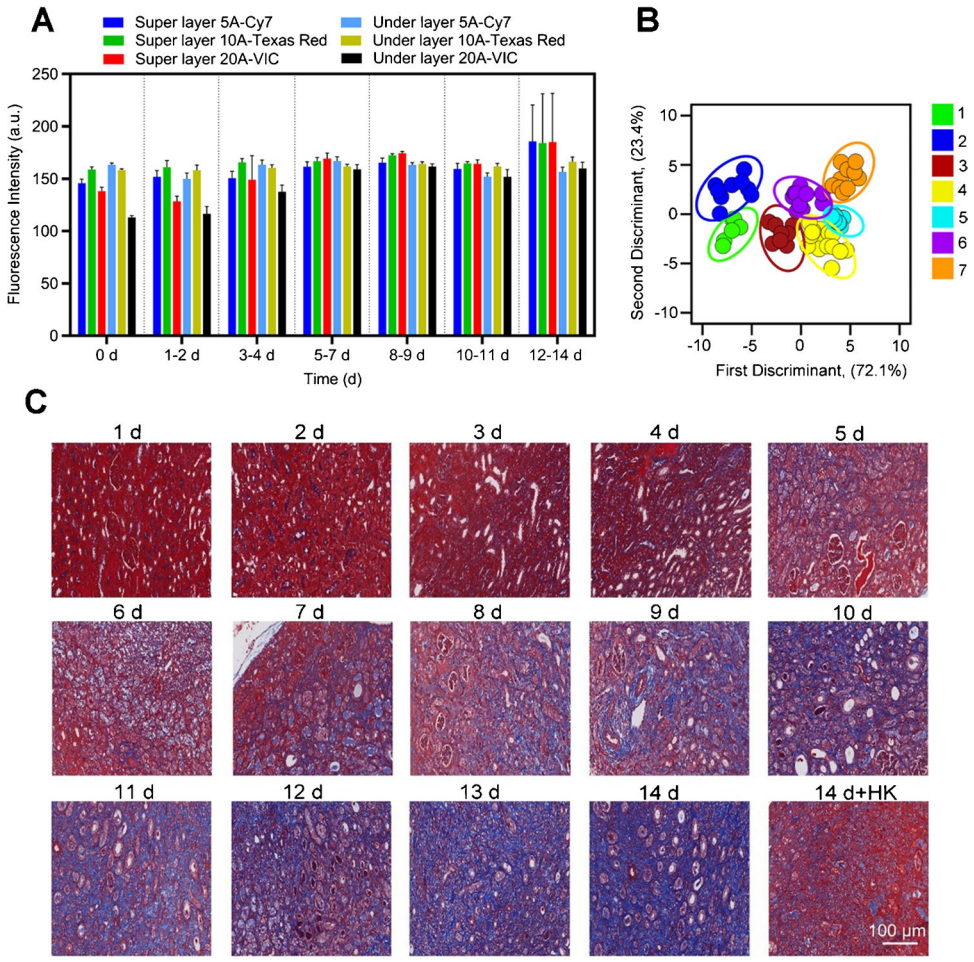

Fig. 4 **A** Fluorescence response patterns generated by PDA-PEI/DNAs sensor for identifying the different kidney injury degrees induced by UUO with six DNA signals. **B** LDA score for discrimination of UUO-induced kidney injury with six DNA signals: 1, control group; 2, UUO model mice ligation for 1–2 days; 3, UUO model mice ligation for 3–4 days; 4, UUO model mice ligation for 5–7 days; 5, UUO model mice ligation for 8–9 days; 6, UUO model mice ligation for 10–11 days; 7, UUO model mice ligation for 12–14 days. **C** Masson staining imaging of renal tissue from UUO mice for different ligation days. Scale bar: 100 μm

$$Y_1 = 0.912X_1 + 0.805X_2 - 1.118X_3 + 6.271X_4 + 12.471X_5 + 5.435X_6 - 1860.994$$
$$Y_2 = 1.130X_1 + 0.945X_2 - 1.313X_3 + 4.949X_4 + 13.317X_5 + 5.489X_6 - 1822.502$$
$$Y_3 = 0.809X_1 + 1.050X_2 - 1.270X_3 + 6.410X_4 + 12.615X_5 + 6.410X_6 - 2031.469$$
$$Y_4 = 1.000X_1 + 0.800X_2 - 1.166X_3 + 6.867X_4 + 12.512X_5 + 7.121X_6 - 2200.629$$
$$Y_5 = 1.057X_1 + 0.860X_2 - 1.207X_3 + 6.320X_4 + 13.131X_5 + 7.170X_6 - 2231.456$$
$$Y_6 = 1.165X_1 + 0.790X_2 - 1.169X_3 + 5.315X_4 + 13.485X_5 + 6.667X_6 - 2064.167$$
$$Y_7 = 1.506X_1 + 0.636X_2 - 1.191X_3 + 5.323X_4 + 14.047X_5 + 6.933X_6 - 2226.907$$

where Y_1–Y_7 respectively represent the kidney injury process of UUO mice in 0, 1–2, 3–4, 5–7, 8–9, 10–11, and 12–14 days; X_1–X_3 represent the fluorescence intensity of three signal molecules induced by super urine; and X_4–X_6 represent the fluorescence intensity of three signal molecules induced by under urine. Mice kidney tissue samples were collected and imaging was performed in a digital section scanner after Masson staining. With the increase of ligation days, the blue area (the formation of collagen fibers) gradually increased (Fig. 4C). In order to visually display the area of kidney tissue fibrosis, Image Pro Plus pathological image analysis software was used to calculate the fibrotic region of Masson staining. The relative area of kidney tubular interstitial fibrosis increased from 1 to 14 ligation days, suggesting a gradual deepening of kidney damage (Fig. S29). Indeed, the relative area of renal tubular interstitial fibrosis in different days of UUO mice was basically consistent with the progress of kidney damage recognized by the sensor.

Finally, in order to investigate the protective effect of HK capsule on kidney injury in UUO model mice, HK capsule was administered continuously for 14 days in UUO mice. The specific values of 6 signals induced by urine in the HK capsule administration group were shown in Table S8. At the same time, the signal values induced by urine were brought into the previously constructed discriminant function and 7 values could be obtained for each group of urine, among which the largest signal value represented its belonging group. As shown in Table S9, fluorescence values of mice administered with HK capsule were all classified as Y_5 group, indicating that the injury degree was consistent with that of ligated mice for 8–9 days. What was noteworthy was that the relative area was reduced to about 40% after administration of HK capsule, which effectively proved that HK capsule improved the process of renal fibrosis (Fig. S12). Both Masson staining and relative area of renal tubular interstitial fibrosis results showed that the degree of renal fibrosis was reduced after HK capsule administration, which proved that HK capsule could effectively improve kidney injury of UUO model mice. In general, pathological section was highly consistent with those discriminant analysis results, validating the accuracy of the PDA-PEI/DNAs sensor in monitoring and evaluating the process of kidney injury.

Discrimination of the clinical samples of diabetic nephropathy

The clinical samples of diabetic nephropathy were used to further verify the reliability and accuracy of the constructed sensor. Three signal molecules were induced to dissociate after the addition of the sensor to the clinical samples of diabetic nephropathy, which led to the occurrence of special fluorescent response pattern (Table S10). The mean values of the three signal molecules induced by different degrees of injury in urine showed significant differences (Fig. 5A), illustrating the difference in the charge of proteins in urine with the progress of injury. In addition, the fitting parameters of PCA model were $R^2 = 0.924$, $Q^2 = 0.873$, respectively. According to the PLS-DA and LDA analysis results, all the samples were obviously divided into four groups: normal group, microproteinuria, macroproteinuria and non-diabetic nephropathy (Fig. 5B and C), which were fully consistent with clinical classification, indicating the accuracy and reliability of the constructed sensor. Values of precision, sensitivity and selectivity were equal to 1.00 and accuracy of 100% showed good discriminative power (Table S11). The four discriminant functions were as follows:

$$Y_1 = 58.938X_1 + 114.767X_2 - 0.635X_3 - 8622.86$$
$$Y_2 = 52.601X_1 + 107.440X_2 - 0.609X_3 - 7418.806$$
$$Y_3 = 55.350X_1 + 107.895X_2 - 0.579X_3 - 7620.6$$
$$Y_4 = 56.140X_1 + 111.745X_2 - 0.626X_3 - 8102.492$$

where Y_1–Y_4 respectively denote the normal group, microproteinuria, macroproteinuria and non-diabetic nephropathy, and X_1–X_3 represent the fluorescence intensity of three signal molecules. Thus, the PDA-PEI/DNAs sensor could also realize the grouping of complex urine and be in accordance with the development stage of clinical diabetic nephropathy, which further verifies the potential application of sensor in clinical diagnosis of the progress of kidney injury.

In order to illustrate the advantages of PDA-PEI/DNAs sensor in identification of kidney injury, a comparison of our work with some existing works [39, 42] are tabulated in Table S12. Compared with traditional kidney injury detection methods, PDA-PEI/DNAs complex can identify the progress of kidney injury via two-dimensional amplification instantaneously and accurately. Significantly, the difference of size and charge of urinary protein could provide a new method to identify the progression of various types of kidney injury. Besides, PDA-PEI/DNAs sensor formed by non-covalent bonding can provide a new method for rapid identification of particle size and charge differences of whole proteins in complex urine samples. However, the feasibility of the method has been demonstrated in cisplatin-induced AKI model, UUO model and the clinical samples

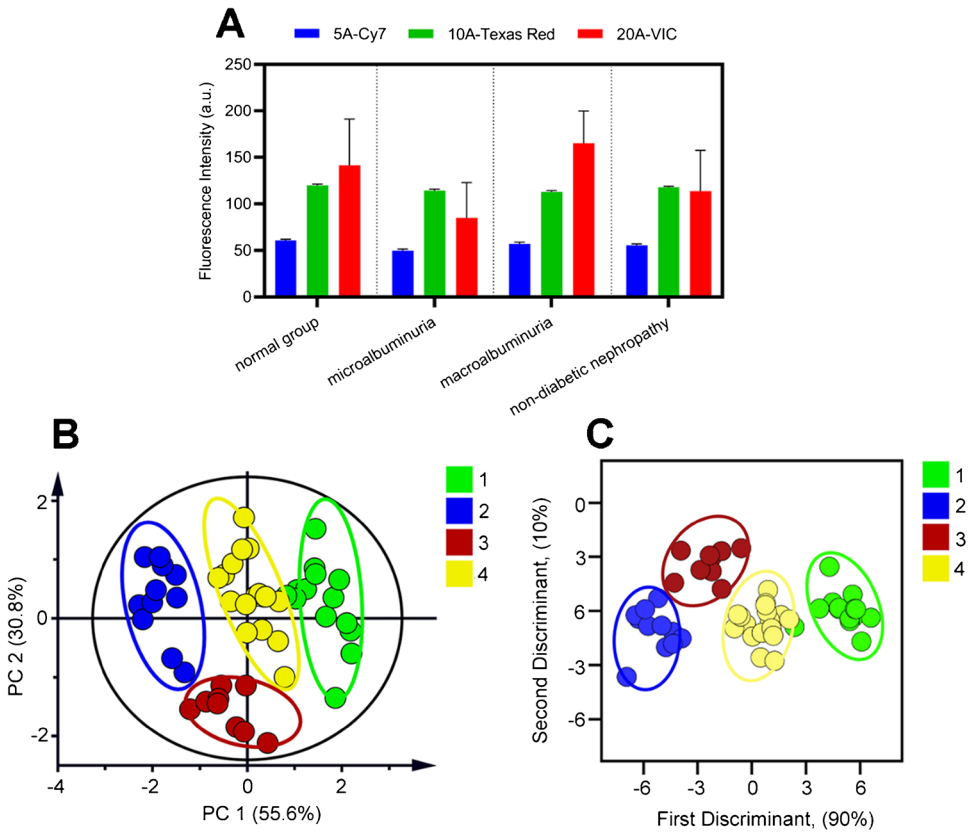

Fig. 5 **A** Fluorescence response patterns generated by PDA-PEI/DNA sensor array for identifying the different kidney injury degrees in clinical samples of diabetic nephropathy. Two-dimensional PLS-DA score plot (**B**) and LDA score plot (**C**) for discrimination of clinical samples of diabetic nephropathy: 1, normal group; 2, microalbuminuria; 3, macroalbuminuria; 4, non-diabetic nephropathy

of diabetic nephropathy, a large number of clinical samples are still needed to confirm that urinary protein particle size and size can be used as novel markers for the development and progression of kidney injury.

Conclusion

In this study, PDA-PEI/DNAs multichannel biosensor was successfully developed based on the response of the size and charge of urine protein, which was constructed of noncovalent interaction of PDA-PEI and three DNAs, providing an information-rich and unique fluorescence fingerprint response that can identify the progress of kidney injury via two-dimensional amplification instantaneously and accurately. Notably, this strategy has presented a significant application of the PDA-PEI/DNAs biosensor in monitoring and evaluating the various kidney injury model including cisplatin-induced AKI model, UUO model, and the clinical samples of diabetic nephropathy via multivariate statistical method. What is more, the protective effects of HK capsule on kidney injury had also been evaluated by the biosensor in urine samples, which was further verified by pathological analysis. Accordingly, the constructed fluorescent fingerprint platform displays a promising approach to discriminate the process of kidney injury, as well as screening the potential kidney-protective drugs.

Supplementary Information The online version contains supplementary material available at https://doi.org/10.1007/s00604-022-05380-9.

Author contribution Xie-an Yu: writing-original draft, methodology, investigation, formal analysis. Lei Zhang: writing—original draft, methodology, investigation. Ran Zhang: formal analysis, data curation. Xuefei Bai: formal analysis, data curation. Yiting Hu: formal analysis, data curation. Ying Zhang: formal analysis, data curation. Yang Wu: data curation. Ziyi Li: data curation. Bing Wang: validation, supervision. Jiangwei Tian: writing—review and editing, validation, supervision, project administration, funding acquisition.

Funding This research was supported by National Natural Science Foundation of China (21775166 and 82104357), Natural Science Foundation for Distinguished Young Scholars of Jiangsu Province (BK20180026), and "Double First-Class" University Project (CPU2018GF06).

Declarations

Conflict of interest The authors declare no competing interests.

References

1. Bellomo R, Kellum JA, Ronco C (2012) Acute kidney injury. Lancet 380(9843):756–766. https://doi.org/10.1016/S0140-6736(11)61454-2
2. Chawla LS, Eggers PW, Star RA, Kimmel PL (2014) Acute kidney injury and chronic kidney disease as interconnected syndromes. N Engl J Med 371(1):58–66. https://doi.org/10.1056/NEJMra1214243
3. Coca SG, Singanamala S, Parikh CR (2012) Chronic kidney disease after acute kidney injury: a systematic review and meta-analysis. Kidney Int 81(5):442–448. https://doi.org/10.1038/ki.2011.379
4. Du B, Yu M, Zheng J (2018) Transport and interactions of nanoparticles in the kidneys. Nat Rev Mater 3:358–374. https://doi.org/10.1038/s41578-018-0038-3
5. Du B, Jiang X, Das A, Zhou Q, Yu M, Jin R, Zheng J (2017) Glomerular barrier behaves as an atomically precise bandpass filter in a sub-nanometre regime. Nat Nanotechnol 12(11):1096–1102. https://doi.org/10.1038/nnano.2017.170
6. Glassock RJ, Warnock DG, Delanaye P (2017) The global burden of chronic kidney disease: estimates, variability and pitfalls. Nat Rev Nephrol 13(2):104–114. https://doi.org/10.1038/nrneph.2016.163
7. Herzog CA, Asinger RW, Berger AK, Charytan DM, Díez J, Hart RG, Eckardt KU, Kasiske BL, McCullough PA, Passman RS, DeLoach SS, Pun PH, Ritz E (2011) Cardiovascular disease in chronic kidney disease. A clinical update from Kidney Disease: Improving Global Outcomes (KDIGO). Kidney Int 80(6):572–86 https://doi.org/10.1038/ki.2011.223
8. Jha V, Garcia-Garcia G, Iseki K, Li Z, Naicker S, Plattner B, Saran R, Wang AY, Yang CW (2013) Chronic kidney disease: global dimension and perspectives. Lancet 382(9888):260–272. https://doi.org/10.1016/S0140-6736(13)60687-X
9. Kubota R, Hamachi I (2015) Protein recognition using synthetic small-molecular binders toward optical protein sensing in vitro and in live cells. Chem Soc Rev 44(13):4454–4471. https://doi.org/10.1039/c4cs00381k
10. Lameire NH, Bagga A, Cruz D, De Maeseneer J, Endre Z, Kellum JA, Liu KD, Mehta RL, Pannu N, Van Biesen W, Vanholder R (2013) Acute kidney injury: an increasing global concern. Lancet 382(9887):170–179. https://doi.org/10.1016/S0140-6736(13)60647-9
11. Le NDB, Yesilbag Tonga G, Mout R, Kim ST, Wille ME, Rana S, Dunphy KA, Jerry DJ, Yazdani M, Ramanathan R, Rotello CM, Rotello VM (2017) Cancer cell discrimination using host-guest "doubled" arrays. J Am Chem Soc 139(23):8008–8012. https://doi.org/10.1021/jacs.7b03657
12. Levey AS, Atkins R, Coresh J, Cohen EP, Collins AJ, Eckardt KU, Nahas ME, Jaber BL, Jadoul M, Levin A, Powe NR, Rossert J, Wheeler DC, Lameire N, Eknoyan G (2007) Chronic kidney disease as a global public health problem: approaches and initiatives - a position statement from Kidney Disease Improving Global Outcomes. Kidney Int 72(3):247–259. https://doi.org/10.1038/sj.ki.5002343
13. Levey AS, James MT (2017) Acute kidney injury. Ann Intern Med 167(9):ITC66–ITC80. https://doi.org/10.7326/AITC201711070
14. Peveler WJ, Landis RF, Yazdani M, Day JW, Modi R, Carmalt CJ, Rosenberg WM, Rotello VM (2018) A rapid and robust diagnostic for liver fibrosis using a multichannel polymer sensor array. Adv Mater 30(28):e1800634. https://doi.org/10.1002/adma.201800634
15. Rana S, Le ND, Mout R, Duncan B, Elci SG, Saha K, Rotello VM (2015) A Multichannel biosensor for rapid determination of cell surface glycomic signatures. ACS Cent Sci 1(4):191–197. https://doi.org/10.1021/acscentsci.5b00126
16. Rana S, Le ND, Mout R, Saha K, Tonga GY, Bain RE, Miranda OR, Rotello CM, Rotello VM (2015) A multichannel nanosensor for instantaneous readout of cancer drug mechanisms. Nat Nanotechnol 10(1):65–69. https://doi.org/10.1038/nnano.2014.285
17. Ricci Z, Cruz D, Ronco C (2008) The RIFLE criteria and mortality in acute kidney injury: a systematic review. Kidney Int 73(5):538–546. https://doi.org/10.1038/sj.ki.5002743
18. Rysz J, Gluba-Brzózka A, Franczyk B, Jabłonowski Z, Ciałkowska-Rysz A (2017) Novel biomarkers in the diagnosis of chronic kidney disease and the prediction of its outcome. Int J Mol Sci 18(8):1702. https://doi.org/10.3390/ijms18081702
19. Yu Z, Cai G, Liu X, Tang D (2021) Pressure-based biosensor integrated with a flexible pressure sensor and an electrochromic device for visual detection. Anal Chem 93(5):2916–2925. https://doi.org/10.1021/acs.analchem.0c04501
20. Zhang K, Lv S, Tang D (2019) Novel 3D printed device for dual-signaling ratiometric photoelectrochemical readout of biomarker using λ-exonuclease-assisted recycling amplification. Anal Chem 91(15):10049–10055. https://doi.org/10.1021/acs.analchem.9b01958
21. Sparrow HG, Swan JT, Moore LW, Gaber AO, Suki WN (2019) Disparate outcomes observed within Kidney Disease: Improving Global Outcomes (KDIGO) acute kidney injury stage 1. Kidney Int 95(4):905–913. https://doi.org/10.1016/j.kint.2018.11.030
22. Saha K, Agasti SS, Kim C, Li X, Rotello VM (2012) Gold nanoparticles in chemical and biological sensing. Chem Rev 112(5):2739–2779. https://doi.org/10.1021/cr2001178
23. Xu Q, Zhang Y, Tang B, Zhang CY (2016) Multicolor quantum dot-based chemical nose for rapid and array-free differentiation of multiple proteins. Anal Chem 88(4):2051–2058. https://doi.org/10.1021/acs.analchem.5b03109
24. Zhang WR, Parikh CR (2019) Biomarkers of acute and chronic kidney disease. Annu Rev Physiol 81:309–333. https://doi.org/10.1146/annurev-physiol-020518-114605
25. Qiu Z, Shu J, Liu J, Tang D (2019) Dual-channel photoelectrochemical ratiometric aptasensor with up-converting nanocrystals using spatial-resolved technique on homemade 3D printed device. Anal Chem 91(2):1260–1268. https://doi.org/10.1021/acs.analchem.8b05455
26. Liu Z, Liu S, Zhou L et al (2012) Effects of HuangKui capsules on glibenclamide pharmacokinetics in rats. J Ethnopharmacol 139(1):1–5. https://doi.org/10.1016/j.jep.2011.03.043
27. Mao ZM, Shen SM, Wan YG et al (2015) Huangkui capsule attenuates renal fibrosis in diabetic nephropathy rats through regulating oxidative stress and p38MAPK/Akt pathways, compared to α-lipoic acid. J Ethnopharmacol 173:256–265. https://doi.org/10.1016/j.jep.2015.07.036
28. Hu Y, Yu XA, Zhang Y et al (2020) Rapid and sensitive detection of NGAL for the prediction of acute kidney injury via a polydopamine nanosphere/aptamer nanocomplex coupled with DNase I-assisted recycling amplification. Analyst 145(10):3620–3625. https://doi.org/10.1039/d0an00474j
29. Jiang Y, Shi M, Liu Y et al (2017) Aptamer/AuNP biosensor for colorimetric profiling of exosomal proteins. Angew Chem Int Ed Engl 56(39):11916–11920. https://doi.org/10.1002/anie.201703807
30. Bian X, Lu Z, van Kollenburg G (2020) Ultraviolet-visible diffuse reflectance spectroscopy combined with chemometrics for rapid discrimination of Angelicae Sinensis Radix from its four similar herbs. Anal Methods 12(27):3499–3507. https://doi.org/10.1039/d0ay00285b
31. Badaró AT, Garcia-Martin JF, López-Barrera MDC, Barbin DF, Alvarez-Mateos P (2020) Determination of pectin content in orange peels by near infrared hyperspectral imaging [published online ahead of print. Food Chem 323:126861 https://doi.org/10.1016/j.foodchem.2020.126861

32. Bello A, Bianchi F, Careri M, Giannetto M, Mori G, Musci M (2007) Multivariate calibration on NIR data: development of a model for the rapid evaluation of ethanol content in bakery products. Anal Chim Acta 603(1):8–12. https://doi.org/10.1016/j.aca.2007.09.037
33. Zhang Y, Yu XA, Hu YT, Bai XF, Zhang R, Lu M, Sun JH, Tian JW, Yu BY (2020) A polydopamine-polyethyleneimine/quantum dot sensor for instantaneous readout of cell surface charge to reflect cell states. Sensors Actuators B Chem 324https://doi.org/10.1016/j.snb.2020.128696
34. Zhao C, Zuo F, Liao Z, Qin Z, Du S, Zhao Z (2015) Mussel-inspired one-pot synthesis of a fluorescent and water-soluble polydopamine-polyethyleneimine copolymer. Macromol Rapid Commun 36(10):909–915. https://doi.org/10.1002/marc.201500021
35. Zhong Z, Jia L (2019) Room temperature preparation of water-soluble polydopamine-polyethyleneimine copolymer dots for selective detection of copper ions. Talanta 197:584–591. https://doi.org/10.1016/j.talanta.2019.01.070
36. Yu XA, Bai X, Zhang R et al (2021) A nanosensor for precise discrimination of nephrotoxic drug mechanisms via dynamic fluorescence fingerprint strategy. Anal Chim Acta 1160:338447. https://doi.org/10.1016/j.aca.2021.338447
37. Weng J, Wang Y, Zhang Y, Ye D (2021) An activatable near-infrared fluorescence probe for in vivo imaging of acute kidney injury by targeting phosphatidylserine and caspase-3. J Am Chem Soc 143(43):18294–18304. https://doi.org/10.1021/jacs.1c08898
38. Cheng P, Chen W, Li S, He S, Miao Q, Pu K (2020) Fluoro-photoacoustic polymeric renal reporter for real-time dual imaging of acute kidney injury. Adv Mater 32(17):e1908530. https://doi.org/10.1002/adma.201908530
39. Huang J, Li J, Lyu Y, Miao Q, Pu K (2019) Molecular optical imaging probes for early diagnosis of drug-induced acute kidney injury. Nat Mater 18(10):1133–1143. https://doi.org/10.1038/s41563-019-0378-4
40. Farid DMd, Zhang L, Rahman CM, Hossain MA, Strachan R (2014) Hybrid decision tree and naïve Bayes classifiers for multi-class classification tasks. Expert Syst Appl 41:1937–1946. https://doi.org/10.1016/j.eswa.2013.08.089
41. Cuadros-Rodríguez L, Pérez-Castaño E, Ruiz-Samblás C (2016) Quality performance metrics in multivariate classification methods for qualitative analysis. TrAC, Trends Anal Chem 80:612–624. https://doi.org/10.1016/j.trac.2016.04.021
42. Yao C, Chen Y, Zhao M, et al (2021) A bright, renal-clearable NIR-II brush macromolecular probe with long blood circulation time for kidney disease bioimaging [published online ahead of print. Angew Chem Int Ed Engl https://doi.org/10.1002/anie.202114273